## Title

Quantitative In Vivo HR-pQCT Imaging of 3D Wrist and Metacarpophalangeal Joint Space Width in Rheumatoid Arthritis



## Journal

Annals of Biomedical Engineering, 41(12)

## ISSN

0145-3068

## Authors

Burghardt, Andrew J
Lee, Chan Hee
Kuo, Daniel
et al.

## Publication Date

2013-12-01

## DOI

10.1007/s10439-013-0871-x

Peer reviewed

Published in final edited form as:
*Ann Biomed Eng*. 2013 December ; 41(12): . doi:10.1007/s10439-013-0871-x.

# Quantitative In Vivo HR-pQCT Imaging of 3D Wrist and Metacarpophalangeal Joint Space Width In Rheumatoid Arthritis

**Andrew J. Burghardt**[1], **Chan Hee Lee**[1,2], **Daniel Kuo**[1], **Sharmila Majumdar**[1], **John B. Imboden**[3], **Thomas M. Link**[1], and **Xiaojuan Li**[1]

[1] Musculoskeletal Quantitative Imaging Research Group, Department of Radiology & Biomedical Imaging, University of California, San Francisco; San Francisco, CA USA

[2] Division of Rheumatology, Department of Internal Medicine, NHIC Ilsan Hospital, Goyang-si, Gyeonggi-do, South Korea

[3] Department of Medicine, University of California, San Francisco and Division of Rheumatology, San Francisco General Hospital; San Francisco, CA USA

## Abstract

In this technique development study, high-resolution peripheral quantitative computed tomography (HR-pQCT) was applied to non-invasively image and quantify 3D joint space morphology of the wrist and metacarpophalangeal (MCP) joints of patients with rheumatoid arthritis (RA). HR-pQCT imaging (82μm voxel-size) of the dominant hand was performed in patients with diagnosed rheumatoid arthritis (RA, N=16, age:52.6±12.8) and healthy controls (CTRL, N=7, age:50.1±15.0). An automated computer algorithm was developed to segment wrist and MCP joint spaces. The 3D distance transformation method was applied to spatially map joint space width, and summarized by the mean joint space width (JSW), minimal and maximal JSW (JSW.MIN, JSW.MAX), asymmetry (JSW.AS), and distribution (JSW.SD) – a measure of joint space heterogeneity. *In vivo* precision was determined for each measure by calculating the smallest detectable difference (SDD) and root mean square coefficient of variation (RMSCV%) of repeat scans. Qualitatively, HR-pQCT images and pseudo-color JSW maps showed global joint space narrowing, as well as regional and focal abnormalities in RA patients. In patients with radiographic JSN at an MCP, JSW.SD was two-fold greater versus CTRL ($p$<0.01), and JSW.MIN was more than two-fold lower ($p$<0.001). Similarly, JSW.SD was significantly greater in the wrist of RA patients versus CTRL ($p$<0.05). *In vivo* precision was highest for JSW (SDD: 100μm, RMSCV: 2.1%) while the SDD for JSW.MIN and JSW.SD were 370 and 110μm, respectively. This study suggests that *in vivo* quantification of 3D joint space morphology from HR-pQCT, could improve early detection of joint damage in rheumatological diseases.

### Keywords

HR-pQCT; rheumatoid arthritis; hand, bone, image processing; joint space width; computed tomography

**Corresponding author:** Andrew J. Burghardt Musculoskeletal Quantitative Imaging Research Group Department of Radiology & Biomedical Imaging University of California, San Francisco QB3 Building, Suite 203 1700 4th St San Francisco, CA 94158 Tel: +1 (415) 514-9658 Fax: +1 (415) 514-9656 andrew.burghardt@ucsf.edu.
Chan Hee Lee chanheell@gmail.com Daniel Kuo dankuo@gmail.com Sharmila Majumdar sharmila.majumdar@ucsf.edu John B. Imboden jimboden@medsfgh.ucsf.edu Thomas M. Link thomas.link@ucsf.edu Xiaojuan Li xiaojuan.li@ucsf.edu

## Introduction

Rheumatoid Arthritis (RA) is an autoimmune disease associated with synovial inflammation, articular cartilage damage, and bone erosion adjacent to joints. In the absence of treatment, RA can ultimately lead to debilitating joint damage with functional limitations and deformity. Clinical studies of RA progression and therapeutic intervention utilize radiography to assess joint damage, including cortical erosions and joint space narrowing (JSN). Most commonly, joint health status is evaluated by standard radiography using a semi-quantitative ordinal scoring system [42]. However, radiographs have limited sensitivity to visualize progression of joint damage, which typically takes a year or longer to manifest. Due to its projectional nature, radiographs may not be adequate for detecting early changes in bone and joint morphology. More recently computerized quantitative approaches to measure joint space width (JSW) have been developed to provide continuous measures of joint space geometry [34,35]. While these techniques represent a major advance for clinical research in RA, common confounders related to radiographic superposition remain a challenge for computerized methods applied to 2D imagery, as they do for semi-quantitative scoring systems. Therefore there is a need for more sensitive quantitative tools that detect early RA-related changes in juxta-articular bone and can determine efficacy early in the course of treatment [13].

High-resolution peripheral quantitative computed tomography (HR-pQCT) is a promising non-invasive imaging method for *in vivo* 3D characterization of human bone [4,19]. With an isotropic voxel size of 82 μm (130 μm spatial resolution), this technology permits quantification of bone density and microstructure in the appendicular skeleton [7,25,27,28]. Although the primary application of this technology has been for the purposes of understanding skeletal development [11,20], aging [4,9,12,19,26], and fracture risk [5,37,40,43] in the context of bone metabolic disorders, recently HR-pQCT has been utilized to image bone affected by inflammatory diseases [16,17,38,39,44]. To date these studies have provided qualitative and semi-quantitative grading of the 3D appearance of the juxta-articular bone surfaces of the metacarpophalangeal (MCP) joint, including the prevalence and scale of erosions and osteophytes. Additionally, quantitative 3D analysis of periarticular cancellous bone density and microstructure has been evaluated in the epiphyses of the distal metacarpal and proximal first phalanx [17] using a protocol adapted directly from methods applied in the distal radius for evaluating bone quality and fracture risk [21]. While bone erosions are a hallmark of RA and are important for monitoring the response to treatment, changes in cartilage are believed to be more predictive of functional outcomes in RA [1,23]. The development of high fidelity imaging biomarkers that reflect early changes in both bone and cartilage associated with inflammatory processes has the potential to accelerate the clinical assessment of treatment efficacy in patients and the evaluation of new therapies in clinical trials.

In this technique feasibility study, HR-pQCT was applied to non-invasively image the MCP and wrist joints of patients with established RA of variable severity, and healthy controls. Automated image processing methods were developed to quantify 3D joint space width, an indirect measure of cartilage morphology. Specifically five quantitative metrics were proposed to characterize joint morphology: (1) joint space volume; (2) the mean three-dimensional joint space width; (3) an estimate of the minimal joint space width; (4) joint space heterogeneity as described by the variance in local joint space widths; and (5) joint space asymmetry. The reproducibility of the technique was determined by repeat acquisitions in a subset of patients.

## Materials and Methods

### Joint Space Width Analysis

The software for the joint space width analysis described below was implemented within the scanner manufacturer's Image Processing Language (IPL v5.08b, Scanco Medical AG, Brüttisellen, Switzerland) and incorporated via extension into their visualization and analysis software (μCT Evaluation v6.0, Scanco Medical AG, Brüttisellen, Switzerland) for routine use by a trained operator. The automated image processing chain is comprised of four primary stages, and described in the following sections. In the first stage, the individual joint of interest is identified. For the MCP this is done semi-automatically, while the wrist joints are identified automatically at a later stage. In the second stage, the mineralized structure is extracted and the periosteal surface is detected for each individual bone comprising the MCP or wrist joint of interest. Next, the individual joint space volumes of interest (VOI) are automatically segmented using morphological erosion/dilation and connectivity procedures. In the final stage, a map of local joint space widths are generated for the joint space VOI. Each stage is described in detail in the following sections, and demonstrated schematically for the MCP in Figure 1.

**Separation of individual joints (Figure 1A)—**In the initial step the individual joint of interest is identified semi-automatically (MCP) or automatically (wrist). For the MCP joints, this simply involves drawing an inclusive circular contour around the proximal and distal extents of the metacarpal and phalanx, respectively. The contour is then interpolated across the intermediate slices, incorporating the joint. Extraction of the mineralized bone structure from the grayscale image data uses an approach adapted from the standard trabecular bone analysis methods developed for imaging the distal radius [22]: a Laplace-Hamming filter, which effectively smoothes the image and enhances edges, is applied to the grayscale data and a fixed global threshold (40% of the maximum possible grayscale value) is applied to discretize the bone and background phases. In contrast, the individual joints of the wrist – radioulnar (RU), radioscaphoid (RS), and radiolunate (RL) – are identified automatically following the binarization step, according to the respective volumes of their constituent bones and anatomic location. This approach assumes the radius is the largest bone in the scanned region and that the proximal margins of the three articulating bones (within the scanned region) are in order proximal to distal: ulna, lunate, scaphoid. Analogously, the metacarpal and phalanx for each individual MCP joint are distinguished according to their position along the distal-proximal axis.

**Periosteal surface segmentation (Figure 1B)—**The periosteal surface was automatically identified for each bone on an individual basis using a series of 3D erosion/dilation steps to close the cortical shell and selection of the contiguous extra-osseal background to fill the medullary space. This process has been described in detail elsewhere [6,8] and results in accurate masks of the individual periosteal surfaces.

**Joint space segmentation (Figure 1C)—**The periosteal masks for the two constituent bones in the joint of interest are next used to segment the articular joint space. First, the surfaces are jointly dilated a sufficient distance to overlap (20 pixels, 1.64 mm), thereby closing the joint space. Any residual voxels in the joint space that are not contiguous with the background are then removed. Next the connected bone and joint space object is eroded back to the original boundary, maintaining a filled joint space. An initial segmentation of the joint space is obtained by subtracting the original periosteal masks from this object. The joint space VOI identified in this final step is used to calculate the morphometric parameters described in the following section.

**Joint space morphometry (Figure 1D)—**The joint space mask derived in the previous step is the basis for calculating the joint space analysis parameters described below (Table 1). Joint space volume (JSV) is calculated using simple voxel-counting of all voxels comprising the masked region. Joint space morphology is quantified based on the direct 3D distance transformation technique [18]: maximal diameter spheres are fit in the background space of the segmented mineralized bone volume (*i.e.* the joint space), resulting in a map of local width values. The histogram of the width map is computed for the region of interest defined by the joint space mask. From this distribution of widths, the mean joint space width (JSW) is defined as the arithmetic mean of the distribution. Similarly the standard deviation of the histogram (JSW.SD) is calculated to characterize the heterogeneity of the joint space. The minimal and maximal JSW (JSW.MIN and JSW.MAX, respectively) are simply calculated as the minimal and maximal values of the joint space histogram. Finally, joint space asymmetry (JSW.AS) was defined as the ratio of JSW.MAX and JSW.MIN, such that the greater the value, the greater the joint asymmetry.

## Patient Study

To evaluate the feasibility of applying the image processing techniques and quantitative measures described in the previous sections, a pilot study was performed in a cohort of patients with established RA and healthy controls [38]. Sixteen patients (RA, age: 52.6±12.8 yrs, 81% female) who fulfilled the 1987 American College of Rheumatology (ACR) classification criteria for RA were recruited for the study. Seven healthy women (CTRL, 50.1±15.0 yrs, 100% female) who had no history of diagnosed rheumatoid diseases were studied as controls. The RA group was 25% Caucasian, 56% Hispanic, and 19% Asian, while the CTRL group was 57% Caucasian and 43% Asian. Mean BMI was significantly greater for the RA group (28.6± 4.9 *vs.* 23.6±5.5, $p < 0.05$), however the groups were not different in terms of mean height or age. The average disease duration for the RA group was 91±85 months, with 81% of subjects having RF-positive and 81% CRP-positive labs. The RA cohort had a recent history of treatment that included DMARDS (94%), DMARDS + Anti-TNF (38%), and glucocorticoids (56%). The local institutional review board for human research approved the design of the study, and written informed consent was obtained from all subjects prior to participation.

**Radiography—**Hand radiographs for the RA patients were accessed from our institutional picture archiving and communication system (PACS) and jointly read by a rheumatologist (CHL) and musculoskeletal radiologist (TML). The van der Heijde modified Sharp method was used to score the images with the individual joint-specific scores [42]. For the purposes of this study, only the JSN component of the Sharp/van der Heijde scores (ranging from 0 to 4) corresponding to the joints analyzed by HR-pQCT were considered individually. The erosion component to the score was disregarded.

**HR-pQCT Imaging—**The MCP joints of all subjects were imaged in a clinical HR-pQCT system (XtremeCT, Scanco Medical AG, Brüttisellen, Switzerland) on the side with manifest disease (RA subjects) or on the dominant side (healthy control subjects). The wrist was also imaged in a subset of patients (RA n=16, CTRL n=3) to study the radiocarpal and radioulnar joints. To minimize radiation dose and scan time, separate acquisitions were performed for the MCP and wrist sites. Due to geometric constraints of the scanner gantry, two different carbon fiber casts were used to immobilize the subject's forearm, for either scan site (Figure 2). For the MCP acquisition, the subject's forearm was fixed in a palm-down orientation within a custom carbon-fiber cast designed at our institution. The wrist acquisition was performed in the standard forearm cast provided by the manufacturer with the hand in a thumb-up orientation [29]. A single dorsal-palmar projection image of the hand/wrist was acquired to define the tomographic scan region for each position (Figure 3). For

the MCP this region was centered at the apex of the third MCP and extended 13.53 mm in the distal and proximal directions (330 slices total). For the wrist, the mid-point of the radial endplate was used as an anatomical reference position with the scan region extending 8.54 mm in the distal direction and 18.52 mm in the proximal direction (330 slices total). The wrist position was selected such that the proximal-most 110 slices corresponded to the standard location (9.5 mm proximal to the mid-point of the radial endplate) for imaging bone quality described in the osteoporosis literature [4,19]. At each site, three sequential tomographic acquisitions were required to cover the 27.06 mm length (330 slices) along the superio-inferior axis. Each 330-slice scan required 8.2 minutes (total scan time: 16.4 minutes for MCP and wrist acquisitions) with an effective dose of approximately 12.6 μSv for each site. The reconstructed images are 1536 × 1536 pixels in size and span a 12.6 cm field of view (FOV), resulting in 82 μm isotropic voxels [15] with a true spatial resolution of approximately 130 μm [10,41]. To assess the reproducibility of the joint space analysis parameters, repeat acquisitions for the MCPs were performed for two RA subjects. The subject was completely removed from the scanner and immobilization device between repeat measurements. Image quality and subject motion was evaluated by two trained observers for each of the three stacks acquired per site, according to a scoring system established for distal radius and tibia HR-pQCT imaging [32]. Individual joints were excluded from the analysis if any portion of the metacarpal or phalangeal joint surfaces fell outside the 330-slice scan range, or if either surface spanned slices from a stack with grade 4 or worse image quality.

**Statistics—**The precision error of each joint space parameter was pooled over three MCP joints (2nd to 4th) measured with repositioning. The root mean square coefficient of variation (RMSCV%) of all paired exams for either site was determined, and the smallest detectable difference (SDD) related to this error was calculated as follows [3,24]:

$$SDD = 1.96 * SD_{diff} \quad (1)$$

Where $SD_{diff}$ is the standard deviation of the differences between repeat measurements for each parameter.

Mean and standard deviations for RA patients (RA) and healthy controls (CTRL) were calculated for all joint space parameters on a joint-specific basis. Additionally, mean morphological measures from MCP joints with an individual non-zero Sharp/van der Heijde JSN score were calculated and compared to the pooled means for the CTRL group. Between group differences were evaluated using Student's t-test with the level for significance set to $p = 0.05$. Statistical tests were performed in JMP (version 9.0.3, SAS Institute Inc., Cary NC).

## Results

Representative images of the MCP and wrist acquisitions for a healthy control and representative RA patient(s) are presented in Figures 3 and 4, respectively, demonstrating the joint space segmentation and morphological quantification. For the MCP, Figure 3 illustrates how variable joint morphology is represented by the individual parameters: a patient with global JSN which is reflected by a lower joint volume, mean JSW, minimal and maximal JSW, while the heterogeneity and asymmetry are comparable to the Normal subject (Figure 3B); a patient with pronounced, but asymmetric JSN as indicated by the high JSW.AS and JSW.SD values, and low mean JSW (Figure 3C); a patient with moderate joint subluxation associated with high maximal JSW, asymmetry, and heterogeneity values, but relatively normal volume and mean JSW (Figure 3D).

### Image Analysis Performance

A total of 72 MCP joints were available for analysis: the scan region covered MCP2 and MCP3 of all 23 subjects, while sufficient coverage of MCP4 was found for 21 subjects. Five scans adequately covered MCP5, however the data are not presented here due to the small number. Of the 72 total joints analyzed, 58 were found to have suitable image quality (81%), while 14 were excluded due to severe motion artifacts (19%). This led to the complete exclusion of three subjects where motion affected all joints in the hand. Of the 58 joints with acceptable image quality, the joint space was successfully segmented for 56 cases (97%). For the unsuccessful cases, the segmentation failed due to localized complete loss of intra-articular space resulting in direct contact between the metacarpal head and phalangeal cup. For this scenario a coarse semi-automatic circling of the metacarpal was used to distinguish the individual bones, which were otherwise processed identically. This task required less than five minutes of operator time.

For the wrist, a total of 57 radiocarpal or radioulnar joints (19 subjects) were available for analysis. Of these, 18 joints from 6 subjects were excluded due to poor image quality related to motion (32%). The joints of one additional subject were excluded due to carpal fusion and severe osteophytosis. For the remaining 36 joints (12 subjects), the joint spaces were successfully segmented for 30 cases (83%), while six required minor semi-manual intervention to separate the individual bones (17%). As for the MCP, this required less than five minutes of operator time.

### Reproducibility

Both subjects with repeat MCP scans had three MCP joints (MCP 2-4) covered by the scan region, for a total of six joints with repeat measurements. The precision results, pooled across all MCP joints, are summarized in Table 1. Both subjects had minor to moderate image quality degradation due to motion artifacts in at least one scan (75% grades 2 or 3), with one MCP2 joint grade 4. The smallest detectable difference for measuring joint volume was 12.2 $mm^3$. Metric indices had a precision of 120 μm or less, with the exception of the minimal JSW, which had an SDD of 370 μm. The lowest relative precision was found for the asymmetry scalar, JSW.AS (RMSCV 13.9%).

### Morphologic differences between RA patients and healthy controls

The group- and joint-wise summary statistics for the full cohort are reported in Table 2. At MCP2, RA patients had significantly narrower JSW.MIN compared to the control group (−22%, $p < 0.05$). Differences did not reach statistical significance for other parameters. At the wrist, JSW.SD of the radiolunate and radioulnar joints was significantly greater for RA patients compared to CTRL ($p < 0.05$). In addition, the minimal JSW was significantly lower in the radioulnate joint ($p < 0.01$), and maximal JSW was significantly greater for the radiolunate joint of RA patients ($p < 0.05$). Joint asymmemtry was significantly great in both the radiolunate and radioulnar joints ($p < 0.05$)

Of the 72 MCP joints analyzed by HR-pQCT, seven joints from four patients (all female) received a non-zero individual Sharp/van der Heijde JSN score. This included four joints with a score of 3 and one each for scores 1, 2, and 4. When pooled together and compared to the pooled results of the CTRL group (Table 3), the RA joints with radiographic JSN had two-fold greater joint space heterogeneity ($p < 0.01$) and less than half JSW.MIN ($p < 0.001$). Joint asymmetry was also significantly greater in the RA group ($p < 0.05$) and substantially more variable. Mean JSW and volume were not statistically different.

## Discussion

In this technique feasibility study we have described an image processing approach to automatically quantify 3D joint space morphology of the wrist and metacarpophalangeal joints affected by inflammatory disease. Furthermore we characterized the *in vivo* precision of these measures for the MCP by repeat acquisitions in a small subset of subjects. The principle outcome of this study was the establishment of analysis methods that are robust across a broad range of morphologies and disease states. The analysis method performed well for normal joints as well as rheumatoid joints with significant changes including large erosions, subluxation, and significant joint space narrowing. Finally, the precision results provide an initial guideline to inform the design of future clinical imaging studies of rheumatoid arthritis.

There are several advantages of this new technique that could significantly benefit future rheumatology research. The use of 3D imaging and analysis techniques avoids the inherent limitations of measuring three dimensional surface features from a 2D projection image, including radiographic superposition, poor contrast of the joint margin, and significant asymmetry [33]. Furthermore, mapping 3D joint space distances provides the opportunity to characterize joint morphology beyond a simple measure of average JSW. In addition to joint space volume and the mean, minimal, and maximal widths, we can also describe the distribution of widths using the standard deviation of the JSW histogram. As illustrated in Figure 3, this metric reflects overall variability in local joint space widths. Using this collection of parameters it is then possible to differentiate global versus regional changes in joint space morphology, something not possible with an ordinal JSN score, but may have important functional implications.

Although only six MCP joints from our RA cohort had a non-zero individual Sharp/van der Heijde score for JSN, the affected joints were significantly associated with high joint space width heterogeneity and asymmetry, but not abnormal mean width. This observation supports the concept that distilling joint morphology into a single average JSN score or metric disregards variable manifestations of joint pathologies, including global narrowing, focal narrowing, asymmetry, and subluxation. In the future it will be of particular interest to investigate the relationship between these individual morphological features and functional outcome measures in controlled prospective studies.

Greater joint space heterogeneity was also observed at the wrist for the RA cohort. This difference was statistically significant despite the lack of radiographic evidence of JSN in this cohort – only one of the nine RA subjects with acceptable quality wrist images had a non-zero individual Sharp score for JSN at the wrist. This difference remained significant after exclusion of the one subject with radiographic JSN, suggesting that 3D morphological measures derived from HR-pQCT images may be more sensitive to changes in joint morphology, compared to traditional scores based on 2D radiography.

In general the mean JSW values from our cohort were comparable in magnitude to JSW values calculated from digital radiographs [31,34]. Precision error for mean JSW measured from HR-pQCT was comparable to what has been reported previously for automated 2D analysis of radiographs – approximately 100 μm [35]. Whereas the *relative* precision of JSW.SD was considerably higher than mean JSW (10.4% vs. 2.1%), the *absolute* SDD was 100 μm or less for both measures. The precision error for JSW.MIN was substantially higher than for the other metrics (SDD: 370 μm, RMSCV: 12.5%). likely indicating that measurement of the minimal joint width is more sensitive to motion artifacts. This is not unexpected given that JSW.MIN is inherently a focal measure, in contrast to the summary statistical parameters calculated over a volume (*e.g.* mean JSW, JSW.SD).

From a technical perspective, the observations of this study recommend several specific protocol changes that would minimize challenges associated with patient motion and scan positioning. The scanner acquires 110-slice stacks (9.02 mm) simultaneously. For longer coverage, multiple tomographic orbits are required, and subject motion can lead to artifactual discontinuities between consecutive 110-slice stacks. Therefore centering the hand scan on the middle of the joint space of the second or third MCP occasionally resulted in these artifacts intersecting the joint surface. While images with severe artifacts were excluded from analysis according to a standard image quality criterion, moderate stack boundary artifacts could still affect the depiction of joint morphology. Changing the scan position such that the distal-most slice of the first 110-slice stack is positioned immediately distal to the endosteal margin of the third phalanx, should avoid localization of discontinuities across the joint surfaces of the second and third MCP. Additionally this could make it possible to acquire two stacks with coverage of MCP2-4, instead of three, thereby reducing scan time, radiation dose, and the incidence of motion. Since the completion of this pilot study, standard positioning guidelines have been proposed by the *Study GrouP for XTrEme-CT* (SPECTRA Group) [2]. We believe these recommendations will greatly reduce the number of images excluded due to poor image quality. Nevertheless, subject motion is a recognized challenge for collecting high quality image data using this system [14,30,32,36]. In particular, we found that the wrist joint was highly susceptible to motion artifacts, with one third of our scans ultimately excluded due to poor quality. Our experience from this pilot study suggests that the standard forearm cast is not well suited for immobilization of the wrist joint. Therefore the development of an improved immobilization solution will be a high priority for planning future studies.

It is important to acknowledge that this study was limited to a demonstration of the feasibility of using HR-pQCT and the described automatic JSW analysis software to quantitatively study joint morphology in the hand and wrist. We have not tested the accuracy of the proposed JSW measures nor provided a robust clinical validation. Furthermore, while precision was reported for a total of six MCP joints from two patients, reliable precision data requires more degrees of freedom in a broader range of subjects. As mentioned previously, improved immobilization and acquisition procedures should improve precision errors; therefore new reproducibility experiments will be necessary for valid interpretation of clinical findings and reliable study design. Nevertheless, the preliminary reproducibility data and observations from the use of this technique in our pilot population are encouraging indications that this method could provide reliable measures of joint morphology.

Several other limitations to this study should be acknowledged. Foremost, the number of subjects was limited, particularly in the control population. Our RA cohort was relatively heterogeneous with respect to their disease status, duration, and treatment history. Accordingly only six joints in the RA cohort had identifiable JSN by traditional radiographic assessment. Furthermore, the CTRL and RA groups were not balanced in terms of racial background, gender, and body size. As such, the results can only suggest feasibility of the technique described. Acceptable clinical validation will require formal investigations of how these measures relate to functional outcomes, detailed clinical assessment of joint status, and cross-sectional differences in clinically relevant populations. Furthermore, the availability of HR-pQCT systems is currently limited to a modest number of research institutes, with dedicated resources and personnel to operate. Translation to broader use in clinical research will require further evidence that HR-pQCT add greater dissemination of the technology and efforts to standardize the acquisition and analysis, and establish appropriate reference data. It remains to be seen whether the technology will mature to the point that it becomes practical and cost-effective for routine clinical use.

In summary, we have presented an automatic image analysis technique to measure 3D joint space morphology from HR-pQCT images of the MCPs and wrist, including simple measures of joint space volume as well as the mean, minimal, and maximal width. We have also proposed the use of the standard deviation of local widths to describe the degree of heterogeneity of the joint space, and the ratio of the minimal and maximal widths to reflect overall asymmetry of the joint. The precision error for the mean JSW was approximately 100μm (2.1%) – comparable to 2D radiographic precision. While a more detailed validation and robust reproducibility analysis of the measured parameters are required, our pilot data suggest this technique could provide new insight into the relationship between 3D joint morphology, function, and disease. Combined with direct assessment of periarticular bone quality, including cortical erosions, and trabecular bone density and morphology, HR-pQCT has the potential to provide a uniquely comprehensive assessment of joint status in clinical research studies of rheumatological diseases, and ultimately a more sensitive means to monitor progression.

## Acknowledgments

The authors would like to thank Melissa Guan, Thelma Munoz, and Gus Del Puerto for coordinating subject recruitment, and translation assistance. Furthermore they thank Dr. Miki Sode, Ph.D. and Steve Rock for the design and construction of the forearm cast used for MCP imaging. This study was supported with funds from a UCSF Academic Senate Grant (XL), NIH R01 AG17762 (SM), and NIH R01 AR060700 (AJB).

## Abbreviations

| | |
|---|---|
| **HR-pQCT** | high-resolution peripheral quantitative computed tomography |
| **RA** | rheumatoid arthritis |
| **CTRL** | control |
| **DMARD** | disease-modifying antrirheumatic drug |
| **MCP** | metacarpophalangeal |
| **RU** | radioulnar |
| **RS** | radioscaphoid |
| **RL** | radiolunate |
| **VOI** | volume of interest |
| **SDD** | smallest detectable difference |
| **JSN** | joint space narrowing |
| **JSV** | joint space volume |
| **JSW** | joint space width |
| **JSW.MIN** | JSW minimum |
| **JSW.MAX** | JSW maximum |
| **JSW.SD** | JSW standard deviation (heterogeneity) |
| **JSW.AS** | JSW asymmetry |

## REFERENCES

1. Aletaha D, Funovits J, Smolen JS. Physical disability in rheumatoid arthritis is associated with cartilage damage rather than bone destruction. Ann Rheum Dis. 2011; 70(5):733–739. [PubMed: 21321002]

2. Barnabe C, Feehan L. High-resolution Peripheral Quantitative Computed Tomography Imaging Protocol for Metacarpophalangeal Joints in Inflammatory Arthritis: The SPECTRA Collaboration. J Rheumatol. 2012; 39(7):1494–1495. [PubMed: 22753808]
3. Bland JM, Altman DG. Statistical methods for assessing agreement between two methods of clinical measurement. Lancet. 1986; 1(8476):307–310. [PubMed: 2868172]
4. Boutroy S, Bouxsein ML, Munoz F, Delmas PD. In vivo assessment of trabecular bone microarchitecture by high-resolution peripheral quantitative computed tomography. J Clin Endocrinol Metab. 2005; 90(12):6508–6515. [PubMed: 16189253]
5. Boutroy S, Van Rietbergen B, Sornay-Rendu E, Munoz F, Bouxsein ML, Delmas PD. Finite element analysis based on in vivo HR-pQCT images of the distal radius is associated with wrist fracture in postmenopausal women. J Bone Miner Res. 2008; 23(3):392–399. [PubMed: 17997712]
6. Buie HR, Campbell GM, Klinck RJ, MacNeil JA, Boyd SK. Automatic segmentation of cortical and trabecular compartments based on a dual threshold technique for in vivo micro-CT bone analysis. Bone. 2007; 41(4):505–515. [PubMed: 17693147]
7. Burghardt AJ, Kazakia GJ, Majumdar S. A local adaptive threshold strategy for high resolution peripheral quantitative computed tomography of trabecular bone. Ann Biomed Eng. 2007; 35(10): 1678–1686. [PubMed: 17602299]
8. Burghardt AJ, Buie HR, Laib A, Majumdar S, Boyd SK. Reproducibility of direct quantitative measures of cortical bone microarchitecture of the distal radius and tibia by HR-pQCT. Bone. 2010; 47(3):519–528. [PubMed: 20561906]
9. Burghardt AJ, Kazakia GJ, Ramachandran S, Link TM, Majumdar S. Age- and gender-related differences in the geometric properties and biomechanical significance of intracortical porosity in the distal radius and tibia. J Bone Miner Res. 2010; 25(5):983–993. [PubMed: 19888900]
10. Burghardt AJ, Pialat JB, Kazakia GJ, Boutroy S, Engelke K, Patsch JM, Valentinitsch A, Liu D, Szabo E, Bogado CE, Zanchetta MB, McKay HA, Shane E, Boyd SK, Bouxsein ML, Chapurlat R, Khosla S, Majumdar S. Multi-center precision of cortical and trabecular bone quality measures assessed by HR-PQCT. J Bone Miner Res. 2012 10.1002/jbmr.1795, 2012/10/18.
11. Burrows M, Liu D, McKay H. High-resolution peripheral QCT imaging of bone micro-structure in adolescents. Osteoporos Int. 2010; 21(3):515–520. [PubMed: 19322507]
12. Dalzell N, Kaptoge S, Morris N, Berthier A, Koller B, Braak L, van Rietbergen B, Reeve J. Bone micro-architecture and determinants of strength in the radius and tibia: age-related changes in a population-based study of normal adults measured with high-resolution pQCT. Osteoporos Int. 2009; 20(10):1683–1694. [PubMed: 19152051]
13. Edmonds J, Lassere M. Imaging damage: scoring versus measuring. J Rheumatol. 2001; 28(8): 1749–1751. [PubMed: 11508574]
14. Engelke K, Stampa B, Timm W, Dardzinski B, de Papp AE, Genant HK, Fuerst T. Short-term in vivo precision of BMD and parameters of trabecular architecture at the distal forearm and tibia. Osteoporos Int. 2012; 23(8):2151–2158. [PubMed: 22143491]
15. Feldkamp LA, Davis LC, Kress JW. Practical cone-beam algorithm. J Opt Soc Am A. 1984; 1:612–619.
16. Finzel S, Englbrecht M, Engelke K, Stach C, Schett G. A comparative study of periarticular bone lesions in rheumatoid arthritis and psoriatic arthritis. Ann Rheum Dis. 2011; 70(1):122–127. [PubMed: 20937672]
17. Fouque-Aubert A, Boutroy S, Marotte H, Vilayphiou N, Lespessailles E, Benhamou CL, Miossec P, Chapurlat R. Assessment of hand trabecular bone texture with high resolution direct digital radiograph in rheumatoid arthritis: A case control study. Joint, bone, spine : revue du rhumatisme. 2012; 79(4):379–383.
18. Hildebrand T, Ruegsegger P. A new method for the model-independent assessment of thickness in three-dimensional images. J Microsc. 1997; 185:67–75.
19. Khosla S, Riggs BL, Atkinson EJ, Oberg AL, McDaniel LJ, Holets M, Peterson JM, Melton LJ 3rd. Effects of sex and age on bone microstructure at the ultradistal radius: a population-based noninvasive in vivo assessment. J Bone Miner Res. 2006; 21(1):124–131. [PubMed: 16355281]

20. Kirmani S, Christen D, van Lenthe GH, Fischer PR, Bouxsein ML, McCready LK, Melton LJ 3rd, Riggs BL, Amin S, Muller R, Khosla S. Bone structure at the distal radius during adolescent growth. J Bone Miner Res. 2009; 24(6):1033–1042. [PubMed: 19113916]
21. Laib A, Hauselmann HJ, Ruegsegger P. In vivo high resolution 3D-QCT of the human forearm. Technol Health Care. 1998; 6(5-6):329–337. [PubMed: 10100936]
22. Laib A, Ruegsegger P. Comparison of structure extraction methods for in vivo trabecular bone measurements. Comput Med Imaging Graph. 1999; 23(2):69–74. [PubMed: 10227372]
23. Landewe R, van der Heijde D. Joint space narrowing, cartilage and physical function: are we deceived by measurements and distributions? Ann Rheum Dis. 2011; 70(5):717–718. [PubMed: 21460405]
24. Lassere M, Boers M, van der Heijde D, Boonen A, Edmonds J, Saudan A, Verhoeven AC. Smallest detectable difference in radiological progression. J Rheumatol. 1999; 26(3):731–739. [PubMed: 10090192]
25. Liu XS, Zhang XH, Sekhon KK, Adams MF, McMahon DJ, Bilezikian JP, Shane E, Guo XE. High-resolution peripheral quantitative computed tomography can assess microstructural and mechanical properties of human distal tibial bone. J Bone Miner Res. 2010; 25(4):746–756. [PubMed: 19775199]
26. Macdonald HM, Nishiyama KK, Kang J, Hanley DA, Boyd SK. Age-related patterns of trabecular and cortical bone loss differ between sexes and skeletal sites: a population-based HR-pQCT study. J Bone Miner Res. 2011; 26(1):50–62. [PubMed: 20593413]
27. MacNeil JA, Boyd SK. Accuracy of high-resolution peripheral quantitative computed tomography for measurement of bone quality. Med Eng Phys. 2007; 29(10):1096–1105. [PubMed: 17229586]
28. Macneil JA, Boyd SK. Bone strength at the distal radius can be estimated from high-resolution peripheral quantitative computed tomography and the finite element method. Bone. 2008; 42(6): 1203–1213. [PubMed: 18358799]
29. MacNeil JA, Boyd SK. Improved reproducibility of high-resolution peripheral quantitative computed tomography for measurement of bone quality. Med Eng Phys. 2008; 30(6):792–799. [PubMed: 18164643]
30. Pauchard Y, Liphardt AM, Macdonald HM, Hanley DA, Boyd SK. Quality control for bone quality parameters affected by subject motion in high-resolution peripheral quantitative computed tomography. Bone. 2012; 50(6):1304–1310. [PubMed: 22445540]
31. Peloschek P, Langs G, Weber M, Sailer J, Reisegger M, Imhof H, Bischof H, Kainberger F. An automatic model-based system for joint space measurements on hand radiographs: initial experience. Radiology. 2007; 245(3):855–862. [PubMed: 17951347]
32. Pialat JB, Burghardt AJ, Sode M, Link TM, Majumdar S. Visual grading of motion induced image degradation in high resolution peripheral computed tomography: impact of image quality on measures of bone density and micro-architecture. Bone. 2012; 50(1):111–118. [PubMed: 22019605]
33. Sharp JT, van der Heijde D, Angwin J, Duryea J, Moens HJ, Jacobs JW, Maillefert JF, Strand CV. Measurement of joint space width and erosion size. J Rheumatol. 2005; 32(12):2456–2461. [PubMed: 16331786]
34. Sharp JT, Angwin J, Boers M, Duryea J, von Ingersleben G, Hall JR, Kauffman JA, Landewe R, Langs G, Lukas C, Maillefert JF, Bernelot Moens HJ, Peloschek P, Strand V, van der Heijde D. Computer based methods for measurement of joint space width: update of an ongoing OMERACT project. J Rheumatol. 2007; 34(4):874–883. [PubMed: 17407243]
35. Sharp JT, Angwin J, Boers M, Duryea J, Finckh A, Hall JR, Kauffman JA, Landewe R, Langs G, Lukas C, Moens HJ, Peloschek P, Strand CV, van der Heijde D. Multiple computer-based methods of measuring joint space width can discriminate between treatment arms in the COBRA trial -- Update of an ongoing OMERACT project. J Rheumatol. 2009; 36(8):1825–1828. [PubMed: 19671820]
36. Sode M, Burghardt AJ, Pialat JB, Link TM, Majumdar S. Quantitative characterization of subject motion in HR-pQCT images of the distal radius and tibia. Bone. 2011; 48(6):1291–1297. [PubMed: 21421091]

37. Sornay-Rendu E, Boutroy S, Munoz F, Delmas PD. Alterations of cortical and trabecular architecture are associated with fractures in postmenopausal women, partially independent of decreased BMD measured by DXA: the OFELY study. J Bone Miner Res. 2007; 22(3):425–433. [PubMed: 17181395]

38. Srikhum W, Virayavanich W, Burghardt AJ, Yu A, Link TM, Imboden JB, Li X. Quantitative and Semiquantitative Bone Erosion Assessment on High-resolution Peripheral Quantitative Computed Tomography in Rheumatoid Arthritis. J Rheumatol. 2013 10.3899/jrheum.120780, 2013/02/19.

39. Stach CM, Bauerle M, Englbrecht M, Kronke G, Engelke K, Manger B, Schett G. Periarticular bone structure in rheumatoid arthritis patients and healthy individuals assessed by high-resolution computed tomography. Arthritis Rheum. 2010; 62(2):330–339. [PubMed: 20112404]

40. Stein EM, Liu XS, Nickolas TL, Cohen A, Thomas V, McMahon DJ, Zhang C, Yin PT, Cosman F, Nieves J, Guo XE, Shane E. Abnormal microarchitecture and reduced stiffness at the radius and tibia in postmenopausal women with fractures. J Bone Miner Res. 2010; 25(12):2572–2581. [PubMed: 20564238]

41. Tjong W, Kazakia GJ, Burghardt AJ, Majumdar S. The effect of voxel size on high-resolution peripheral computed tomography measurements of trabecular and cortical bone microstructure. Med Phys. 2012; 39(4):1893–1903. [PubMed: 22482611]

42. van der Heijde D. How to read radiographs according to the Sharp/van der Heijde method. J Rheumatol. 2000; 27(1):261–263. [PubMed: 10648051]

43. Vico L, Zouch M, Amirouche A, Frere D, Laroche N, Koller B, Laib A, Thomas T, Alexandre C. High-resolution pQCT analysis at the distal radius and tibia discriminates patients with recent wrist and femoral neck fractures. J Bone Miner Res. 2008; 23(11):1741–1750. [PubMed: 18665795]

44. Zhu TY, Griffith JF, Qin L, Hung VW, Fong TN, Au SK, Tang XL, Kwok AW, Leung PC, Li EK, Tam LS. Structure and strength of the distal radius in female patients with rheumatoid arthritis: A case-control study. J Bone Miner Res. 2012 10.1002/jbmr.1793, 2012/10/24.

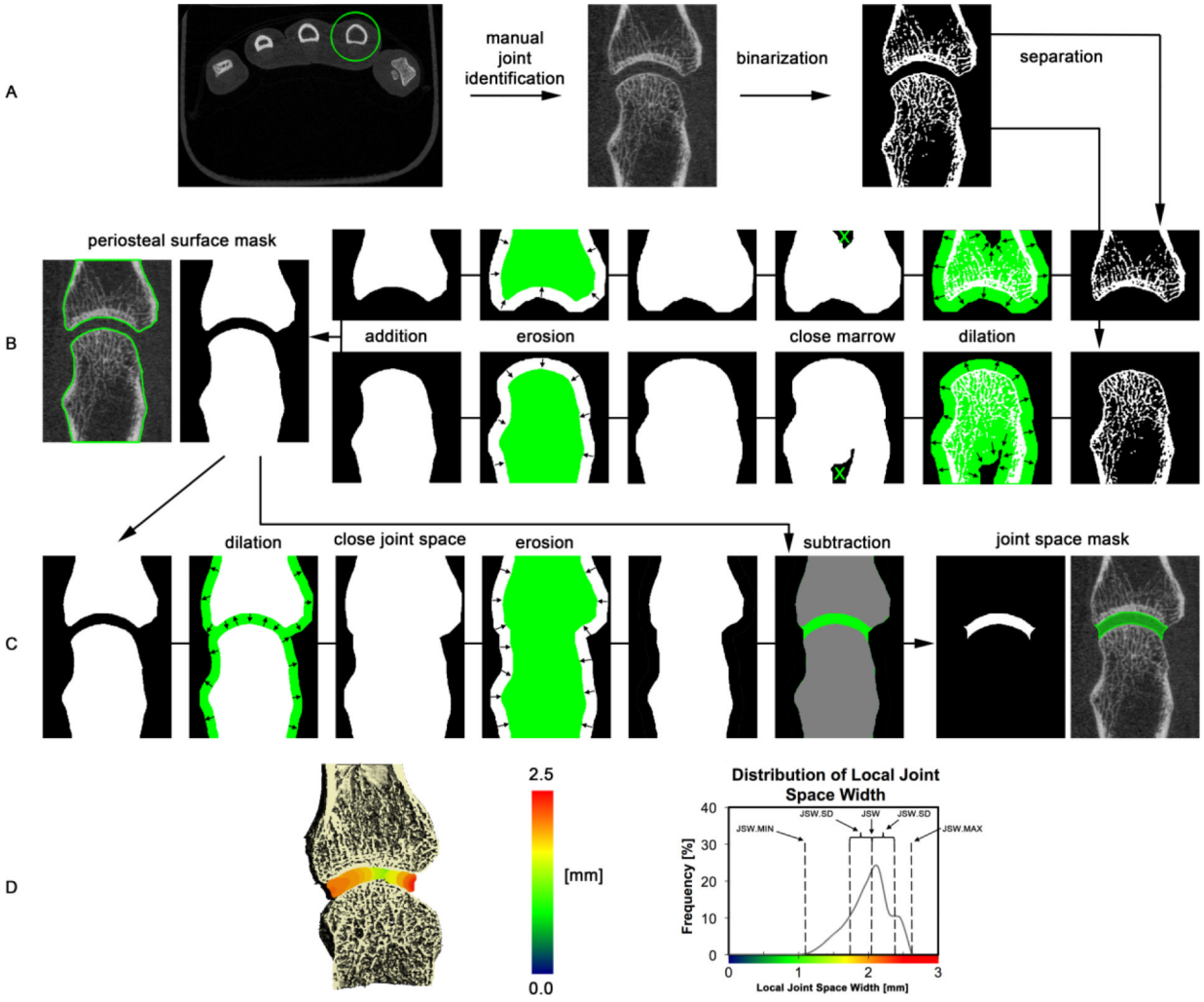


**Figure 1.**

Schematic overview of the image processing steps for the joint space segmentation. In the first step (A), all mineralized bone structures are extracted by thresholding and the individual bones are segmented using the relative supero-inferior position (MCP) or bone size and supero-inferior position (wrist). In the following step the periosteal surfaces are individually identified for each bone in the joint of interest (B). Next, the joint space volume is identified by closing the joint space using dilation/erosion of the juxta-ariticular surfaces followed by subtraction of the original volume contained within the periosteal surface (C). Finally, joint space morphometric parameters are derived from the 3D map of local joint space widths, shown in pseudo-color here for the second MCP of a subject with RA, and corresponding distribution of local joint space widths.

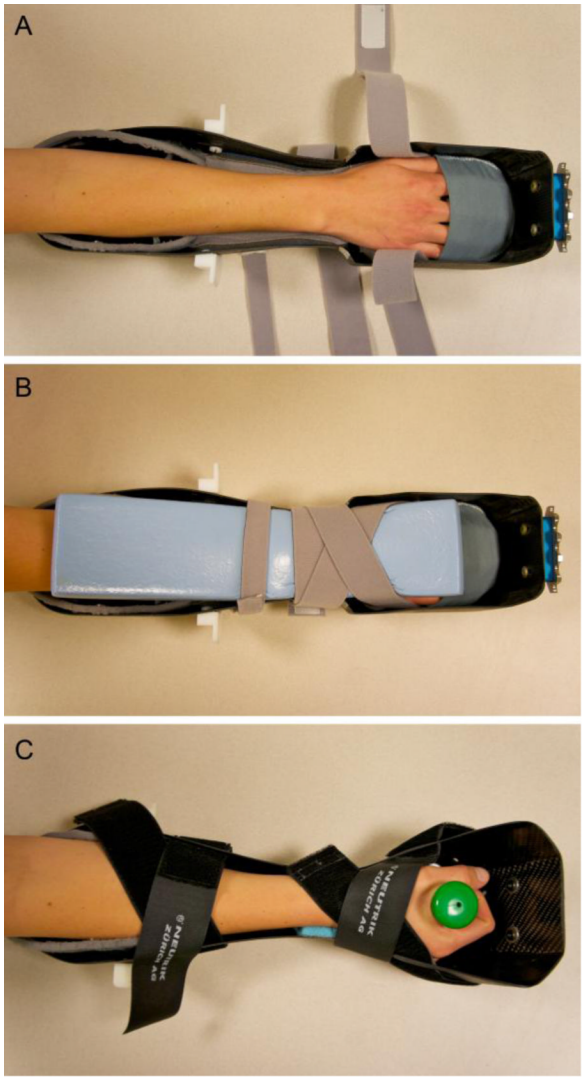


**Figure 2.**
Photographs of the casts used for immobilization of the forearm in the scanner gantry. A palm down orientation is used in a specially designed cast for imaging the second to fourth MCP joints of the hand (A) with the dorsal side compressed via foam and Velcro straps (B). The standard forearm cast provided by the manufacturer was used for imaging the wrist (C).

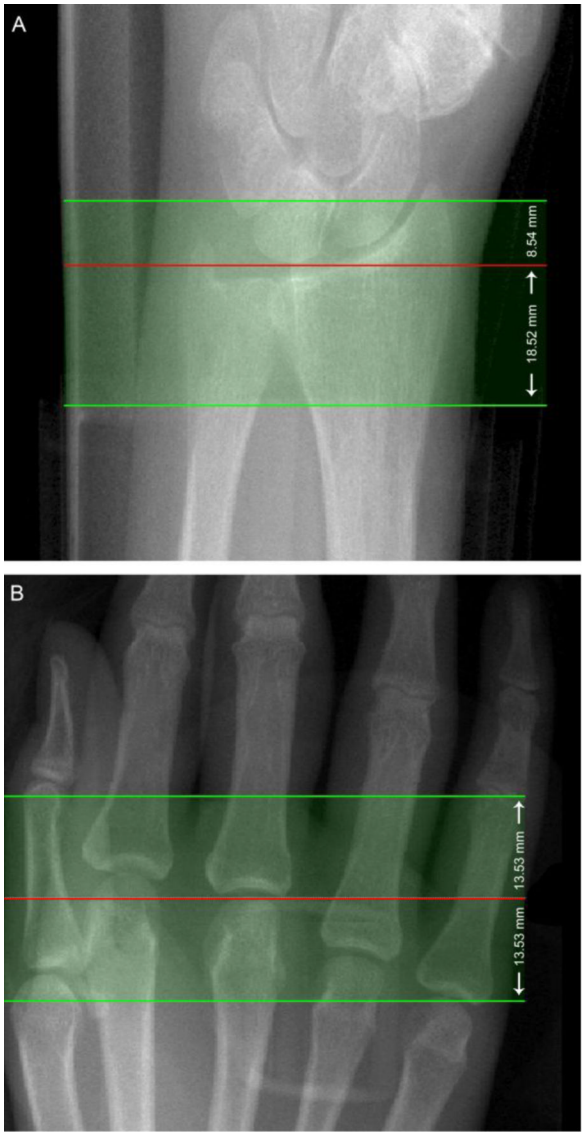


**Figure 3.**

Representative scout radiographs for the wrist (A) and MCPs (B) illustrating the localization for the tomographic acquisition (filled green). For the wrist (A), the operator places the reference line (red) at the inflection in the curvature of the radial endplate with the scanned region (green) extending 8.54 mm distally and 18.52 mm proximally. The final 9.02 mm corresponds to the standard region for scanning the radius in adults for the assessment of bone quality. For the MCPs (B), the reference line (red) is positioned at the distal apex of the 3$^{rd}$ metacarpal, extending 13.53 mm in the proximal and distal directions (B).

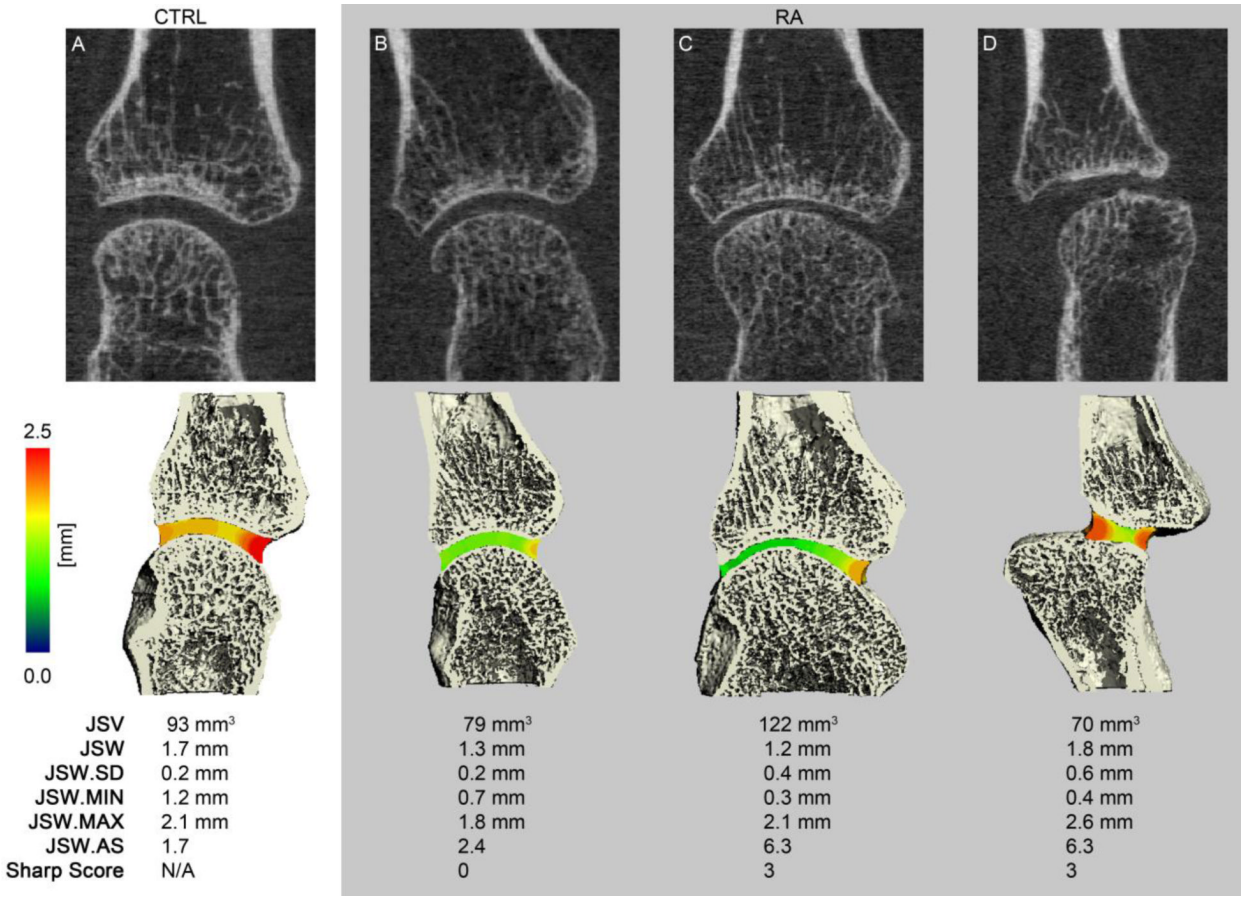


**Figure 4.**

Representative tomographic 2D coronal images of the metacarpal (top), 3D surface reconstructions of the MCP with the local JSW mapped into the joint space in pseudo-color (middle), and corresponding joint space morphometric values (bottom). Shown are a healthy 25 year old individual (A) and three different RA subjects with various joint space abnormalities, including global joint space narrowing (B), joint space heterogeneity and asymmetry (C), and joint subluxation (D).

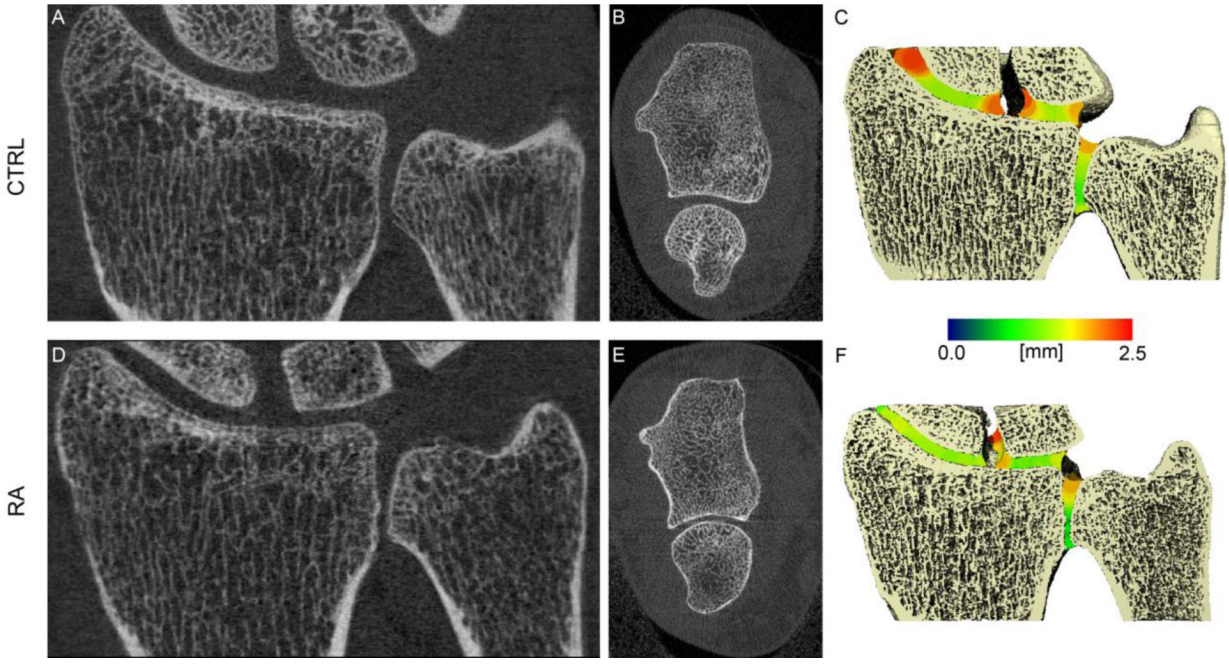


**Figure 5.**

Representative tomographic 2D coronal and axial images of the wrist (left and middle respectively), and 3D surface reconstructions of the wrist with the local JSW mapped into the joint space in pseudo-color (right). Shown is a healthy 25 year old individual (A-C) and a RA subject with various joint space abnormalities, including global joint space narrowing and joint space heterogeneity (D-F).

## Table 1

Joint space analysis parameter descriptions and precision values

| Parameter | Units | SDD (RMSCV%) | Description |
|---|---|---|---|
| JSV | [$mm^3$] | 12.2 (3.5%) | Joint space volume; direct voxel-based measure of the volume of the intra-articular joint space |
| JSW | [mm] | 0.11 (2.1%) | Joint space width; mean of local 3D widths across the joint space |
| JSW.SD | [mm] | 0.07 (10.4%) | Joint space width distribution; standard deviation of local 3D widths across the joint space |
| JSW.MIN | [mm] | 0.37 (12.5%) | Minimal joint space width; Minimal absolute 3D width across the joint space |
| JSW.MAX | [mm] | 0.12 (2.2%) | Maximal joint space width; Maximum absolute 3D width across the joint space |
| JSW.AS | [ ] | 0.92 (13.9%) | Joint space width asymmetry; ratio of the maximal to minimal joint space widths |

## Table 2

Summary of joint space analysis parameters (mean±SD) pooled over all subjects

| Parameter | Units | Joint | | | | | |
|---|---|---|---|---|---|---|---|
| ***MCP*** | | ***MCP2*** | | ***MCP3*** | | ***MCP4*** | |
| | | **CTRL (n=6)** | **RA (n=13)** | **CTRL (n=6)** | **RA (n=13)** | **CTRL (n=5)** | **RA (n=12)** |
| JSV | [$mm^3$] | 109±16 | 117±33 | 111±19 | 122±28 | 89±17 | 91±14 |
| JSW | [mm] | 1.75±0.16 | 1.73±0.25 | 1.60±0.22 | 1.65±0.23 | 1.51±0.25 | 1.53±0.22 |
| JSW.SD | [mm] | 0.24±0.06 | 0.30±0.14 | 0.23±0.03 | 0.26±0.12 | 0.23±0.02 | 0.24±0.07 |
| JSW.MIN | [mm] | 1.27±0.18 | **1.02±0.39**$^{a}$ | 1.12±0.20 | 1.03±0.35 | 1.03±0.20 | 0.99±0.33 |
| JSW.MAX | [mm] | 2.24±0.25 | 2.27±0.22 | 2.03±0.28 | 2.16±0.24 | 1.92±0.22 | 1.99±0.16 |
| JSW.AS | [ ] | 1.78±0.24 | 4.13±6.78 | 1.82±0.11 | 2.58±1.68 | 1.88±0.18 | 2.68±2.6 |

| ***Wrist*** | | ***RL*** | | ***RS*** | | ***RU*** | |
|---|---|---|---|---|---|---|---|
| | | **CTRL (n=3)** | **RA (n=9)** | **CTRL (n=3)** | **RA (n=9)** | **CTRL (n=3)** | **RA (n=9)** |
| JSV | [$mm^3$] | 220±22 | 252±67 | 242±26 | 278±62 | 117±39 | 157±51 |
| JSW | [mm] | 1.80±0.15 | 1.94±0.20 | 1.81±0.16 | 1.84±0.29 | 1.70±0.19 | 1.70±0.26 |
| JSW.SD | [mm] | 0.28±0.06 | **0.39±0.05**$^{a}$ | 0.32±0.03 | 0.32±0.07 | 0.38±0.07 | **0.49±0.07**$^{a}$ |
| JSW.MIN | [mm] | 1.07±0.22 | 0.81±0.38 | 0.98±0.22 | 0.83±0.51 | 0.82±0.08 | **0.45±0.22**$^{b}$ |
| JSW.MAX | [mm] | 2.36±0.07 | **2.61±0.15**$^{b}$ | 2.44±0.14 | 2.51±0.32 | 2.35±0.32 | 2.54±0.21 |
| JSW.AS | [ ] | 2.28±0.48 | **4.24±2.7**$^{a}$ | 2.59±0.79 | 5.37±4.55 | 2.91±0.69 | **8.71±8.90**$^{a}$ |

* **BOLD** indicates statistically significant difference *vs.* CTRL:

$^{c}p < 0.001$

$^{a}p < 0.05$

$^{b}p < 0.01$

## Table 3

Summary of MCP joint space analysis parameters (mean±SD) for RA patients with non-zero Sharp/van der Heijde scored joints and all controls, pooled over all joints.

| Parameter | Units | CTRL (n=17) | RA (n=7) |
|---|---|---|---|
| JSV | [$mm^3$] | 104±19 | 91±39 |
| JSW | [mm] | 1.63±0.22 | 1.46±0.28 |
| JSW.SD | [mm] | 0.23±0.04 | **0.47±0.13**$^{b}$ |
| JSW.MIN | [mm] | 1.15±0.21 | **0.48±0.37**$^{c}$ |
| JSW.MAX | [mm] | 2.07±0.27 | 2.24±0.29 |
| JSW.AS | [ ] | 1.82±0.18 | **8.58±8.40**$^{a}$ |

* **BOLD** indicates statistically significant difference *vs.* CTRL:

$^{a}$ $p < 0.05$

$^{b}$ $p < 0.01$

$^{c}$ $p < 0.001$